Scanning Electron Microscopy

Volume 1985
Number 1 *1985*

Article 7

1-21-1985

Recent Developments in Electrical Microcharacterization Using the Charge Collection Mode of the Scanning Electron Microscope

D. B. Holt
Imperial College of Science and Technology, London

M. Lesniak
Imperial College of Science and Technology, London

SCANNING ELECTRON MICROSCOPY/1985/I (Pages 67-86)
SEM Inc., AMF O'Hare (Chicago), IL 60666 USA

0586-5581/85$1.00+.05

RECENT DEVELOPMENTS IN ELECTRICAL MICROCHARACTERIZATION USING THE CHARGE COLLECTION MODE OF THE SCANNING ELECTRON MICROSCOPE

D. B. Holt* and M. Lesniak

Department of Metallurgy and Materials Science,
Imperial College of Science and Technology,
London, SW7 2BP

(Paper received March 29 1984, Completed manuscript received January 21 1985)

Abstract

There are six distinguishable types of charge collection (CC) signal. Consequently specially designed CC detection systems are needed to obtain e.g. true EBIC and EBIV measurements and make quantitative electrical microcharacterization possible. EBIC and EBIV can arise from fields due to barriers such as p-n junctions or due to changes in doping e.g. p to p+. Materials, defect and device parameters are calculable from these signals. Hot-cold stages are important for temperature dependence studies of contrast, for improving signal to noise ratios and reducing leakage currents. Image processing and pattern recognition methods are vital for rapidly locating and evaluating the information in CC micrographs of large scale circuits. Some recent applications of these techniques to junctions and Schottky barriers in devices, to dislocations and grain boundaries, to microplasmas and to the location of defects in large scale intergration (LSI) devices are presented.

KEY WORDS: Charge collection, Electron beam induced current (EBIC), Electron beam induced voltage (EBIV), β-conductivity, Dislocation contrast, Image processing, Microplasmas

*Address for correspondence:
Department of Metallurgy & Materials Science,
Imperial College, London, SW7 2BP, U.K.

Phone No: 01 589 5111

Introduction

Each mode of the Scanning Electron Microscope operates by transducing into electrical video signals some form of energy into which a part of the incident electron beam energy is dissipated. Electron bombardment of any material that has a low equilibrium density of free charge carriers results in significant additional charge carrier generation. This is because the incident electrons have typically tens of keV energy while the average formation energy of hole-electron pairs, e_i, is about three times the forbidden band gap energy. For example, in silicon e_i = 3.6 eV. Hence in silicon thousands of electron-hole pairs are generated in the energy dissipation volume, a few microns in diameter, for each incident beam electron. The generated carriers constitute an "injected" current given by

$$I_g = G\ I_b \qquad (1)$$

where I_b is the electron beam current and G is the generation factor i.e. the number of electron hole pairs produced for each incident electron. It can be written as

$$G = V_b\ I_b\ (1 - K)/e; \qquad (2)$$

where V_b is the electron beam accelerating voltage and K is the fraction of the incident electrons "backscattered" from the specimen without loss of energy. I_g/e is the number of electron-hole pairs generated per second where e is the charge on an electron.

"Charge collection" is due to the separation of the pairs by an internal, "built-in" field (this is an electron voltaic effect - EVE) or by an externally applied bias (this is the β-conductive effect). The result in either case is that the beam-induced electrons are "collected" by one contact and the holes by a second contact to a specimen. Thus the charge collection (CC) or conductive mode detects currents or voltages. These are already electrical signals, so there is no need to employ transducers for detection. This is one reason that what has misleadingly come to be generally referred to as electron beam induced current microscopy, has tended to be carried out with little thought given to detection (Holt (1981)). The second reason is that, because the numbers of electron-hole pairs generated per

second are much larger than the beam currents, electron beam induced currents (EBIC) are relatively large. Thus any convenient amplifier connected across the specimen can be used for EBIC microscopy e.g. for Si devices. Moreover the practical purpose of such investigations, such as integrated circuit failure mode identification, is often quite adequately served by visual examination of such micrographs (see e.g. Schick (1981, 1985)).

CC Mode Signals and Detection Systems

However there are three signal generating mechanisms: the barrier and bulk electron voltaic effects (EVE's), analogous to the barrier and bulk photovoltaic effects, and the β-conductive effect analogous to the photoconductive effect. Each of these mechanisms can give rise to well-defined signals represented by analytical formulae under two different detection conditions. Thus there are six physically-distinct and mathematically-interpretable types of signal obtainable in the charge collection mode as listed in Table 1. From the measured values of these signals, quantitative values for a wide variety of materials properties and device parameters can be computed. What is unique about these electrical measurements is that they have spatial resolutions of the order of a micron. These techniques are therefore coming to be referred to as electrical microcharacterization.

TABLE 1

Quantitatively Interpretable Types of CC Signal

Mechanism	Forms of Signal	Interpretive References
Barrier electron voltaic effect	I_{sc} (EBIC) V_{oc} (EBIV)	Czaja (1966) Holt (1974) Balk et al (1975) Huang et al (1982).
Bulk electron voltaic effect	I_{sc} (EBIC) V_{oc} (EBIV)	Munakata (1966, 1967a, 1967b). Holt (1974).
β-conductivity	ΔI_β (V_{cc} = const.) ΔV_β (I_{cc} = const.)	Munakata (1968a 1968b, 1969), Gopinath (1970) Gopinath and De Monts De Savasse (1971), Holt(1974).

In order to obtain well-defined signals, to which analytical expressions can be applied, special detection systems are needed. This is primarily because the input characteristics of the detector must meet the particular requirements for that type of signal. It must have a very low input impedance, compared to the specimen to detect short circuit currents Isc. It must have a very large input impedance in order to obtain the open-circuit voltage due to a bulk or barrier EVE. It must provide either constant-current biasing or constant-voltage biasing to the specimen to obtain quantitatively interpretable β-conductivity signals as indicated in Table 1. In addition the detection system must be able to deal with currents, voltages, frequency bandwidths and noise levels of the magnitudes encountered in practice. Biasing, backoff, electronic signal processing and monitoring facilities and a computer interface are desirable features of such a detection system (Lesniak et al (1984)). A block diagram of such a system is shown in Figure 1.

The computer-controlled, beam-chopping and phase lock amplifier system developed by Ourmazd et al (1983b) and Wilshaw et al (1983) is shown in Figure 2. These authors emphasise the importance of fast computer data recording for minimizing the total irradiation time of areas on which measurements are to be made and for obtaining reproducible results.

As little work has yet been done using β-conductivity, attention will be concentrated on the use of true EBIC and Electron Beam Induced Voltage (EBIV) signals, i.e. the CC short-circuit current I_{sc} and the CC open circuit voltage V_{oc}. These provide information of great interest for semiconductor device studies.

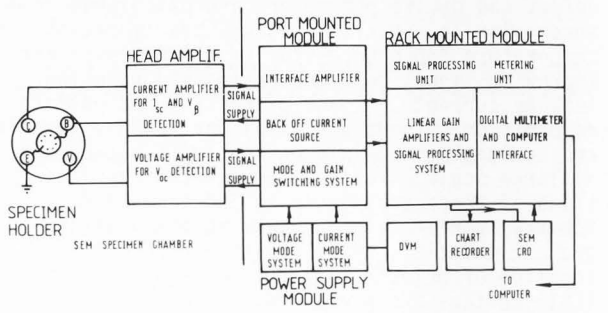

Figure 1. Block diagram of a conductive mode detection system. The port-mounted module fits through a vacuum port on the side of the specimen chamber of a JEOL JSM-35 with the head amplifier inside and the operating controls on a box outside. The power supply is based on rechargeable batteries so high voltage floating biases can be applied across devices and for freedom from a.c. ripple. The rack-mounted module contains final stages of amplification, differentiating, square rooting and filtering facilities and digital and analogue monitoring of signal strengths and operating parameters. A Faraday cup is placed next to the specimen for beam current and diameter determinations. (After Lesniak et al (1984)).

Detection and Interpretation of Bulk and Barrier EVE EBIC and EBIV Signals

The principles of the barrier and bulk electron voltaic effects are illustrated in Figure 3. Whenever the position of the Fermi level alters relative to the conduction and valence band edges, there must be band bending, since in equilibrium the Fermi level (the electrochemical potential of

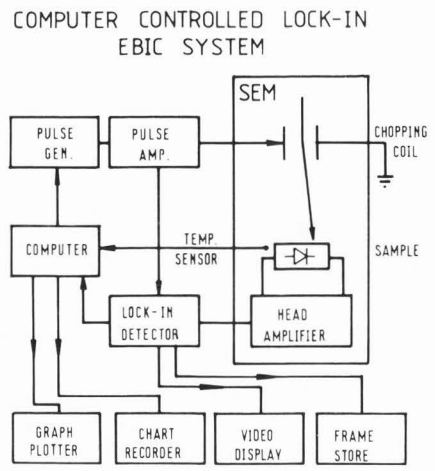

Figure 2. A computer-controlled, lock-in EBIC detection system. (After Ourmazd et al (1983b)).

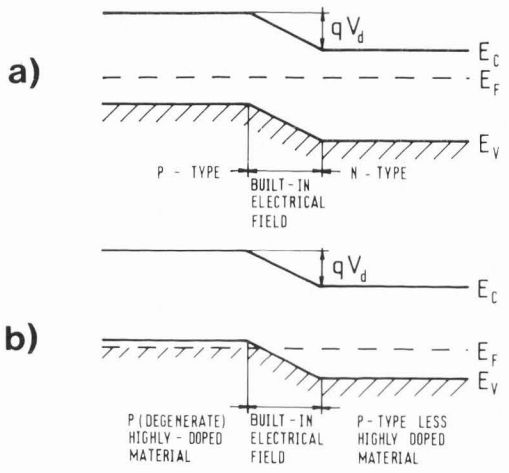

Figure 3. Built-in electric fields in specimens that can produce charge separation i.e. charge collection can occur (a) at barriers such as p-n junctions or (b) bulk regions across which the doping concentration changes markedly. The first gives rise to the barrier electron voltaic effect and the second to the bulk electron voltaic effect (see Table 1) (Holt (1974)).

the carriers) must be constant. That is, there are diffusion potential jumps, V_d, and built-in electrical fields in such regions. Hence at a potential barrier such as a Schottky barrier or a p-n junction (Figure 3(a)) or a "bulk" region of gross doping concentration change such as a p-p$^+$ layer (Figure 3(b)) charge separation will occur. These are the barrier and bulk EVE's respectively. The EVE's generate electromotive forces in the specimen which transfer energy from the incident electron beam to an external circuit to drive the signals. It is not necessary for the specimen to be semiconducting for this to occur. In the case of (semi) insulating specimens the coupling between the separated charges and the contacts may be capacitative. For example, "EBIV" signals can be obtained from extremely high resistivity ZnS platelet crystals (Holt and Culpan (1970)).

Thus not only well-understood detector characteristics but also a knowledge of the specimen equivalent circuit are necessary in order to interpret the contrast in micrographs or the signal strengths measured for quantitative electrical microcharacterization. This becomes a severe problem when the electron beam is incident at a point in the interior of a large-scale integrated circuit. There will be many current paths from the signal generating point to the charge collecting contacts. Many of these paths will be interconnected in complex series and parallel networks. Moreover they may contain active amplifying components such as transistors and logic gates.

To get the most out of the CC mode as applied to Large Scale Integration (LSI) circuits will not be easy, but the prize justifies the effort as will be discussed below.

Analytical Expressions for True EBIC and EBIV

The best understood and most important case is that of the barrier EVE. Specimens containing p-n or heterojunctions or Schottky barriers act as rectifying diodes. The simple drift-diffusion recombination theory for such barriers leads to the well known diode current equation:

$$I_j = I_o \, (\exp(-eV/nkT) - 1) \qquad (3)$$

where I_o is the saturation reverse bias current V is the diode voltage, k is Boltzmann's constant T is the temperature in degrees Kelvin and n is an "ideality" factor, n = 1 corresponds to zero carrier recombination at the barrier. Increasingly larger values of n are characteristic of barriers in ill-developed materials in which recombination-like complications arise.

When the electron beam is incident on a barrier like that in Figure 4(a) the electrons flow to the low, n-side and the holes rise to the p-side. The resultant net charges, -ve on the n-side and +ve on the p-side, forward bias the diode. Consequently a diode forward bias current I_j, tends to flow back in opposition to the charge collection generated current, I_g, as shown in Figure 4(b). Hence the net, externally observable signal current is given by

$$I = I_g - I_j = \eta_{cc} \, G \, I_b - I_o(\exp(eV/nkT) - 1) \qquad (4)$$

where η_{cc} is the charge collection efficiency of the barrier for the particular experimental geometry employed.

The barrier EVE short circuit current is obtained by setting V = 0 in equation (4). This is the true electron-beam induced current (EBIC) signal and is therefore given by:

$$I_{sc} = \eta_{cc} \, G \, I_b \qquad (5)$$

Similarly the open circuit voltage for the barrier EVE, the true electron beam induced voltage (EBIV) signal, is obtained, as first pointed out by Balk et al (1974), by setting I = 0 in equation (4):

$$V_{oc} = (nkT/e) \ln (1 + I_g/I_o) \qquad (6)$$

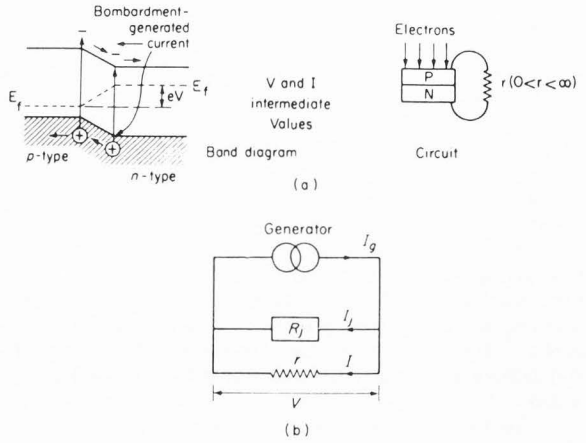

Figure 4. The barrier electron voltaic effect at a p-n junction: (a) the electron beam induced electrons and holes are separated by the built-in field at the junction so that if an input impedance r comparable to the resistance of the specimen is connected externally a current and a voltage will be generated. (b) The beam-induced forward biasing of the junction leads to a junction current I_j flowing back in opposition to the generated current I_g.

Balk et al used this method to obtain the barrier height i.e. the built-in diffusion potential V_d of a p-n junction. This was the maximum value of V_{OC} as the beam current I_b and hence I_g was increased. To apply these equations to particular cases, however, expressions and values that are appropriate for the particular type of barrier and experimental conditions involved must be substituted for the parameters in equations (5) and (6). Some examples of such applications will be given below.

More complete theoretical treatments of EBIC and EBIV signals will be found in Holt (1974), Bresse (1977), Davidson (1977), Davidson and Dimitriadis (1980) and Leamy (1982).

Hot-Cold Stages for EBIC Microcharacterization

It was first reported by Kimerling et al (1977) that the EBIC contrast of defects in Si could be altered by raising the specimen temperature. The principle is that the Fermi level moves from its position near a band edge at low temperatures to the mid-gap position at high, intrinsic-conduction temperatures. Thus in n-type material it can be made to sweep down over the top half of the band gap. As the Fermi level passes through the energy level or levels of a defect they will become less completely electron filled. The defect EBIC contrast should then change. In practice, subsequent workers (Ourmazd and Booker (1979), Ourmazd et al (1983a, 1983b), Lesniak et al (1984)) have found it more valuable to use liquid nitrogen stages to study temperature-dependent contrast at reduced temperatures. This is because changes in dislocation contrast occur below room temperature in Si and because lowering the temperature reduces electrical noise and leakage currents. The latter changes have effects on the quality of micrographs that are often dramatic.

Examples of Applications

The volume of work in this field is now so large that no attempt was made to achieve a complete coverage. Instead certain particular applications in which progress has been very rapid were chosen for presentation here. Even in these topics an exhaustive literature review was not attempted. The most important applications for microelectronic device studies are those to active barriers such as p-n junctions and Schottky barriers.

EBIC Line Scans Across Devices

By scanning the electron beam in a direction at right angles to a p-n junction over a surface normal to the junction as shown in Figure 5 a line scan trace like that in Figure 6 is obtained.

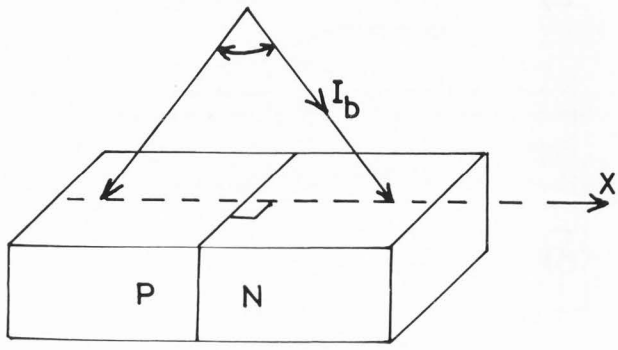

Figure 5. Scanning normal to a p-n junction results in an I signal of such forms as shown in Figures 6 to 8 and 11.

Wittry and Kyser (1965) showed that if (a) surface recombination effects were neglected and (b) the carrier generation was assumed to be spherically symmetric, the variation of the charge collection current, I_{sc}, the true EBIC signal, with x, the distance of the beam impact point from the junction, should have the form:

$$I(x) = I_m \exp(-x/L) \qquad (7)$$

where L is the minority carrier diffusion length in the material on that side of the junction and I_m is the theoretical maximum collection current i.e. the value of I_{sc} (equation (4)) for $\eta_{cc} = 1$ i.e. 100% efficient charge separation and x = 0, i.e. the beam incident on the junction plane.

Good approximations to expression (7) are sometimes found so values of L can be reliably evaluated. By extrapolating back to the junction from straight line portions of the curves in log I(x) plots, the value of I_m can be found. The

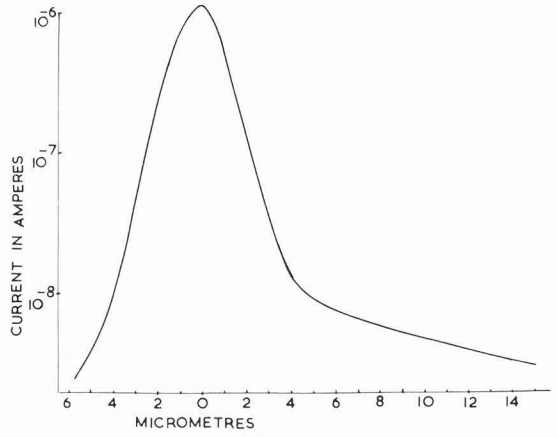

Figure 6. The variation of the true EBIC current with distance from a p-n junction in GaAs (After Holt and Chase (1973)).

value of the charge collection efficiency of the junction is given by

$$\eta_{cc} = I_a/I_m \qquad (8)$$

where I_a is the actual, maximum value of the charge collection I_{sc} current for x = 0 i.e. at the junction.

Several effects were found to complicate the form of I(x). In GaAs Wittry and Kyser (1965) found two exponential terms in the curves on the n-side, which can be seen in Figure 6. Holt and Chase (1973) showed this to be due to short range collection of minority carriers (holes) by diffusion plus long range self detection of infra-red photons by the junction acting as a photovoltaic diode, as assumed by Wittry and Kyser. In scanning across the π (low doped p-type) - p - n+ layers in Si avalanche photodiodes, two exponential decays were found on the π-p side as shown in Figure 7. These were due to the fact that $L_\pi > L_p$.

MacDonald and Everhart (1965) pointed out that if the depletion region at a p-n junction was wider than the resolution of the EBIC technique, a plateau would be observed in the EBIC line scan as shown in Figure 8. By applying a reverse bias to widen the depletion region, the doping can readily be measured if one side is highly conducting and the other is highly resistive. In this common type of junction, the depletion width increases effectively only on the high resistivity side and the width is given by

$$w = \left[\frac{2\varepsilon}{eN_A}(V_r + V_d)\right]^{\frac{1}{2}} \qquad (9)$$

where ε is the dielectric constant, N_A is the impurity concentration (of acceptors, say) on the high-resistivity side of the junction, V_r is the applied voltage and V_D is the diffusion potential (barrier height) of the junction and e is the electronic charge. Their measurements, as shown in Figure 9, followed equation (9) well and gave a value for N_A of 4.7×10^{13} atoms cm^{-3}. The

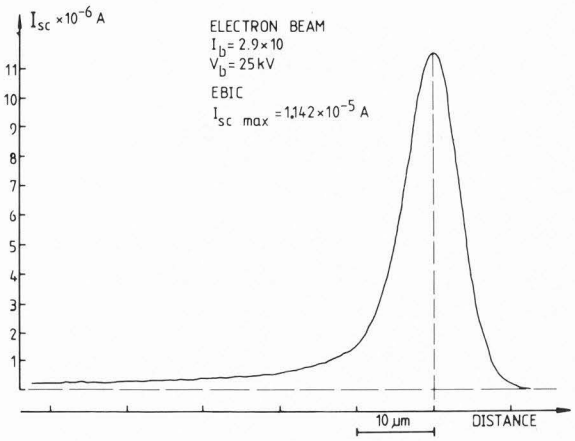

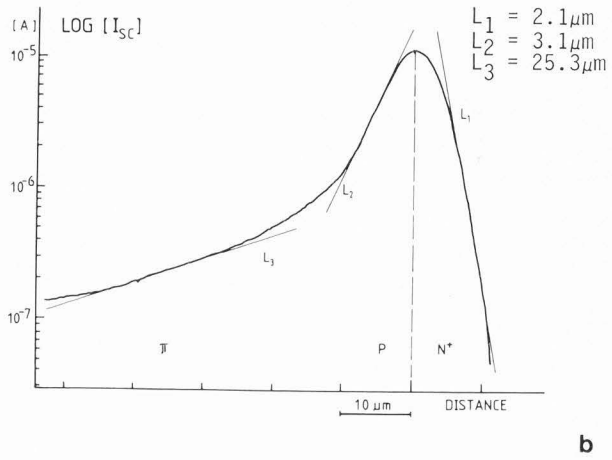

Figure 7. Barrier EVE I_{SC} (true EBIC) line scan through half the thickness of a Si avalanche photodiode (a) linear current and (b) log current plot. The straight line regions in (b) follow equation (7) and the relevant values of the minority carrier diffusion lengths can be obtained for these regions (After Lesniak et al (1984)).

dashed lines are for values of N_A of 10^{13} and 10 10^{14} cm^{-3} and indicate the precision of the method. Schick (1981) developed the use of differentiated EBIC line scans to determine depletion widths as a function of the reverse bias applied to Schottky barriers. The results were similar to those of MacDonald and Everhart (1965) but the spatial resolution was improved by differentiating the signal.

In a study of line scan traces across Si power diodes Davidson et al (1982) found that due to the presence of p^+ p and n n^+ bulk EVE's as well as a p-n barrier EVE as indicated in Figure 10, the EBIC line scans had the three peak form shown in Figure 11. Moreover as can be seen

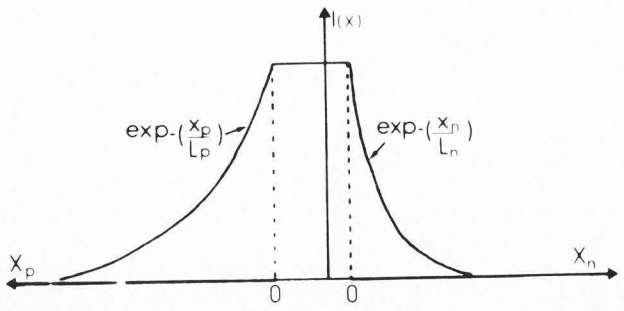

Figure 8. The form of an EBIC line scan across a p-n junction with a resolvable depletion region of width extending from one dotted line to the other. (After Georges et al (1980)).

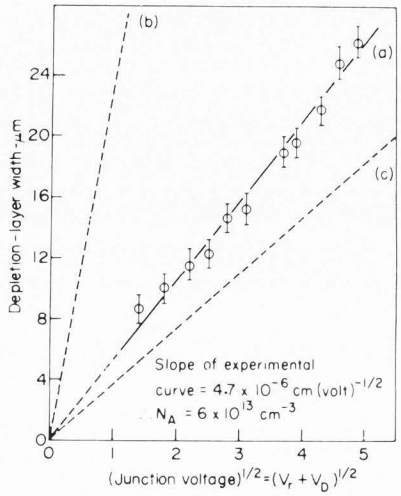

Figure 9. The depletion region width versus the square root of the p-n junction voltage for applied reverse biases V_r. (After MacDonald and Everhart (1965)).

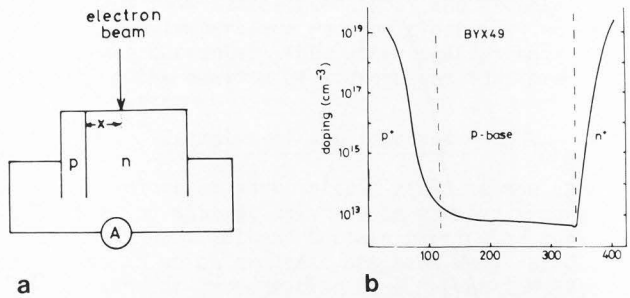

Figure 10. (a) The geometry of line scans across Si power diodes and (b) the doping profile along the linescans of (a) for BYX49 devices. (After Davidson et al (1982)).

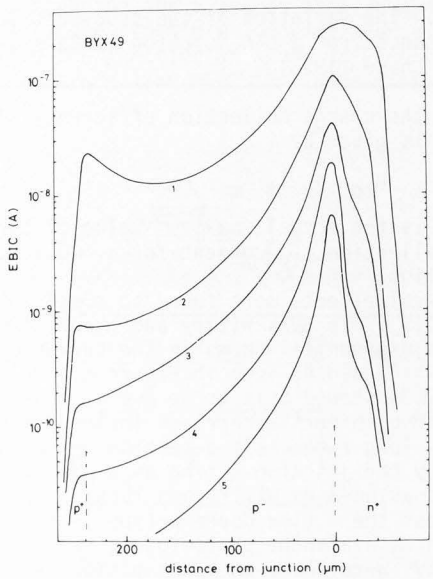

Figure 11. EBIC line scans recorded as shown in Figure 10 for electron beam powers of (1) 11 μW (2) 3 μW (3) 0.9 μW (4) 0.3 μW and (5) 0.1 μW. (After Davidson et al (1982)).

the form of the curves changed markedly with the beam power. In particular the application of equation (7) to the exponential regions of the curves in the p region gives an apparent variation of L with beam power. Davidson et al developed a theory which ascribed this to injection level effects. The essential idea is that if the injected carrier density Δn becomes larger than the equilibrium density p, the recombination statistics may alter e.g. the recombination centres may become "saturated" so the effective recombination time τ would increase. The diffusion length is given by:

$$L = (\tau D)^{\frac{1}{2}} \qquad (10)$$

where D is the diffusion coefficient for the minority carriers. Therefore it would also increase. This would account for the collection of larger currents from greater distances seen in Figure 11.

An obvious alternative is that the combination of the overlapping bulk p^+ p EVE and the barrier p-n EVE produced the observed effect. Such a model was proposed for similar observations on InP p^+ p-n junctions by Marten and Hildebrand (1983). Quantitative studies are necessary to establish the relative importance of the two effects in particular cases.

What were discussed as complicating factors above are, of course, sources of additional information. For example the form of line scans like those in Figure 11 can provide information on the non-uniform doping in the p p^+ and the n n^+ regions as well as on the position and properties of the p-n junction and the material adjacent to it. Further development of interpretive theory for such phenomena is thus desirable. Computer analysis of such signal traces can then be

used for rapid quantitative microcharacterization of specialized device doping profiles.

EBIV Measurements of Schottky Barrier Heights

Huang et al (1982) substituted into equation (6) for the true EBIV signal the specific expression for Schottky barriers to obtain:

$$V_{oc} = n[\phi_B + (kT/e)\ \ln(GI_b/A_d A^* T^2)] \quad (11)$$

where ϕ_B is the Schottky barrier height, A is the diode area and A^* is the Richardson constant. They made measurements on a number of PtSi, Pd_2Si and $TiSi_2$ contacts to silicon, with the beam incident on the metal. They plotted V_{oc} versus the log of the beam current I_b and found straight lines, as shown in Figure 12, to confirm the applicability of equation (11). The slopes gave values for n, the ideality factor for the barriers, of 1.02 for all three. By measuring G, values for ϕ_B were obtained that were in agreement in each case with those obtained from current voltage measurements. Huang et al pointed out that the EBIV method is particularly good for the study of changes in barriers of small heights and they used it to study the effect of annealing Ti on Si as $TiSi_2$ formed in situ as shown in Figure 13.

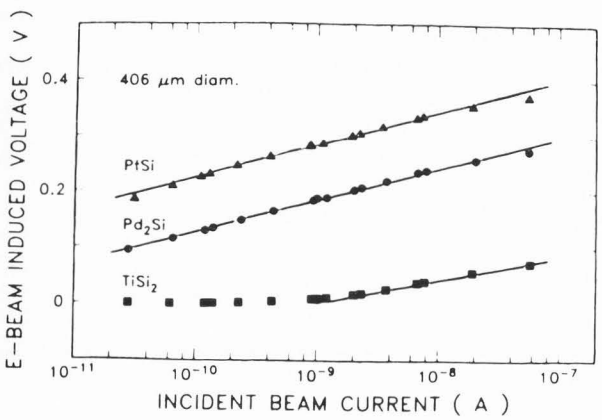

Figure 12. Plots of V_{oc} against log I_b for Si Schottky diodes with PtSi, Pd_2Si and $TiSi_2$ silicide contacts. (After Huang et al (1982)).

If the beam is kept incident on a fixed point at a suitable distance, usually a few times L, from a barrier and chopped at a time t = 0 the EBIC signal will fall from the initial value, I(x) = I(x,0), given by equation (7) as:

$$I(t) = I(0)\ \exp\ (-t/\tau) \quad (12)$$

where τ is the minority carrier lifetime. This method was developed by Zimmermann (1972) for measurements of spatial variations in the value of τ and used e.g. by Hunter et al (1973), Balk et al (1975), Blenkinsop et al (1976), Davidson (1977) and Georges et al (1980).

Quantitative Studies of Electrical Defects

Studies of the electrically active defects in semiconductor materials and devices are of obvious importance for materials assessment, quality control and process validation in production environments. Much of this work is of a qualitative micrographic character. Quantitative studies of defect contrast can provide fundamental data on the properties of defects and this can then be used for the identification of defects seen in testing and inspection.

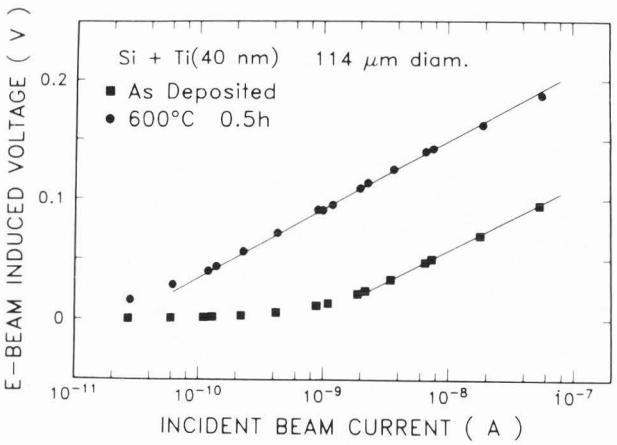

Figure 13. V_{oc} versus log I_b for Si/Ti contacts as deposited and after annealing to allow silicide formation. (After Huang et al (1982)).

There is also great fundamental interest in the electrical and luminescent properties of dislocations in semiconductors. This is due to a combination of developments including (i) the increasing theoretical understanding of the quantum mechanical states arising from the atomic core structure of dislocations (see e.g. Labusch and Schroter (1980), Marklund (1983), Heggie and Jones (1983)), (ii) a substantial body of experimental data on the influence of dislocations on the electrical conductivity and Hall effect in a few materials (Ge, Si, InSb) (Labusch and Schroter (1980), Schroter et al (1980), Schroter (1980)) and the availability of (iii) the atomic resolution TEM technique for determining the atomic core structures and (iv) the SEM, EBIC and cathodoluminescence (CL) modes for observing directly the electrical and luminescence properties of individual dislocations of identifiable types. The latter identification can be done most directly in scanning transmission electron microscope (STEM) microscopes with EBIC or CL facilities or both (Petroff et al (1978), Petroff et al (1980), Fathy et al (1980)). An example of STEM, CL and EBIC micrographs of the same dislocations, taken from the second of these papers, is reproduced in an accompanying review of CL mode dislocation studies (Holt and Saba (1985)).

Interest in this field arose in the 1950's with the observations that small plastic strains sufficed to convert lightly-doped n-type Ge to p-type conduction and that the dislocation density as determined by etch pit counts was the best means of assessing crystal quality. Shockley (1953) pointed out that the cores of dislocations with an edge component, in materials with the diamond crystal structure, would contain atoms bonded to only three nearest neighbours.

The fourth valence electron would be in a broken or "dangling" bond. The "edge states" to which these correspond should interact to give rise to one-dimensional energy bands in the forbidden energy gap.

The details are still partly controversial but it appears now to be agreed that there are two types of states forming narrow energy bands in the gap. The half filled band or filled-and-neighbouring-empty bands near the mid-gap position are thought to be associated with Shockley's dangling bonds. These may well occur only at some type of special site such as a kink in a partial dislocation, however. Shallow levels are drawn out of the valence and conduction bands by the localized deformation potential due to the elastic strain fields of dislocations.

One or more of these dislocation bands, and/or impurities segregated to dislocations, act as recombination centres. These reduce the numbers of hole-electron pairs that can be collected by a p-n junction or Schottky barrier. Consequently the CC signal is reduced locally and so some dislocations appear as dark lines in EBIC micrographs. This means of observation is important because it is the only one that, at present, has the spatial resolution to allow electrical measurements to be made on single dislocations.

A serious problem in all dislocation studies in semiconductors is that of avoiding the effects of impurity segregation into Cottrell atmospheres round the dislocations or into decorating precipitates. These effects dominate in as-grown and device processed material (Holt (1979)).

Dislocation Contrast. Dark dislocation contrast in EBIC micrographs is interpreted as due to enhanced recombination at or near the dislocation (Czaja (1966)). The contrast is defined to be

$$C = (I_B - I_D)/I_B \qquad (13)$$

where I_B and I_D are the BEVE I_{SC} (EBIC) current values for the bulk material i.e. for the beam incident far from any defect, and at the dislocation respectively, as shown in Figure 17(a).

Evidence that impurity segregation and the type and core structure of dislocations are both important in determining the magnitude of the EBIC contrast was provided by comparisons of transmission electron microscope (TEM) and EBIC micrographs. In Figure 14, for example, it is clear that the visible precipitates marked by the arrows in (b) give increased dark contrast in (a). The bright regions flanking the dark lines at the 90° (pure edge) dislocations at B and C were interpreted by Blumentritt et al (1979) as evidence that segregation to the dislocation lines had denuded the surrounding volume of impurity atoms. The 60° dislocation marked A gives rise to no dark contrast in (a) and is not surrounded by a brighter denuded (gettered) zone. Figure 15 concerns a specimen deformed by single slip under constant (creep) stress at low temperatures and strain rates. This type of deformation is known from EPR (electron paramagnetic (or spin) resonance) studies to be essential to introduce clean dislocations that are at least relatively unaffected by impurity segregation (Grazhulis and Osipiyan (1970, 1971), Schmidt et al (1974), Alexander et al (1975)). The arrowed area shows clearly that the two well-separated partial dislocations give rise to EBIC contrast but the stacking fault between them does not. Figure 16 shows a Frank partial dislocation that constitutes the lower boundary of the stacking fault visible as a dark area in the TEM micrograph. This gives dark contrast in the EBIC micrograph where it runs straight along a $\langle 1\bar{1}0\rangle$ direction but it is invisible where it bulges downward in a $\langle 2\bar{1}1\rangle$ direction to the right of point B. Again the stacking fault gives no significant EBIC contrast.

A theory of CC (EBIC) defect contrast was produced by Donalato (1978/79, 1979a, 1979b, 1979c, 1980,1981). This considers dislocations as line sinks for minority carriers. Their effect is represented by introducing a cylinder of radius r round the dislocation line in which the minority carrier lifetime has a value $\tau' < \tau$, the bulk value. Computer simulation was used (e.g. Donalato and Klann 1980) to predict the contrast due to a dislocation, an oxidation-induced stacking fault loop intersecting the surface and a tetrahedral stacking fault, for various values of the incident beam voltage, etc. The results were in good qualitative agreement with micrographic observations. The theory was extended to the case of EBIC contrast profiles in STEM conditions by Donalato (1981). Quantitative measurements of dislocation EBIC resolution and contrast in Si Schottky barrier observations were in agreement with the theory (Toth (1981)).

The original theory represented dislocations as having some characteristic strength or recombination efficiency. Ourmazd and Booker (1979) determined the recombination efficiency which is proportional to the contrast for dislocations at the same distance from the charge collecting barrier. It was found, in the case of edge dislocations, to increase with the percentage of their length that was dissociated into partials. Ourmazd et al (1981) used relative recombination efficiencies to compare the electrical activity of screw and 60° segments of hexagonal dislocation loops in Si.

Recent applications of the theory for the quantitative evaluation of the EBIC contrast of dislocations were reviewed by Donalato (1983a) and this account is followed in this paragraph. The recombination efficiency of a dislocation can be expressed by means of a linear recombination velocity:

$$v = \pi r^2 / \tau' \qquad (14)$$

Kittler and Seifert (1981) introduced a method for obtaining v from experimental data. Pasemann et al (1982) determined the line recombination velocities of numerous 60° dislocations and found that the value for dissociated dislocations was more than twice that for contracted (unit) dislocations, as shown in Figure 17(a), in agreement with the earlier findings of Ourmazd and Booker. If it is assumed that the recombination of minority carriers inside the dislocation cylinder is due to N recombination centres per unit volume of capture cross-section σ, the reduced minority carrier lifetime there can be written as

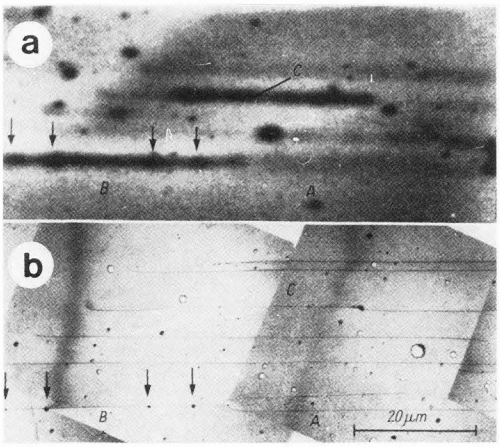

Figure 14. (a) SEM EBIC and (b) high voltage TEM micrographs showing the influence of dislocation type and decoration on EBIC contrast in Si. B and C are heavily decorated 90° dislocations giving rise to strong dark contrast in the EBIC picture whereas the 60° dislocation A has little effect. Contrast due to visible precipitate particles occurs at the arrowed sites. (After Blumentritt et al (1979)).

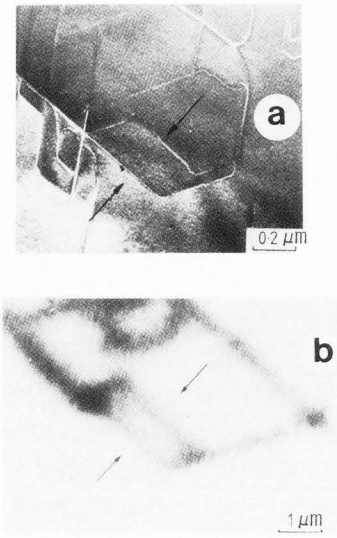

Figure 15. (a) Weak-beam TEM and (b) SEM EBIC micrographs of dislocations in deformed Si. The arrows indicate the widely separated Schockley partial dislocations of a dissociated screw dislocation. There is no EBIC contrast due to the stacking fault between them. (After Ourmazd et al (1983a)).

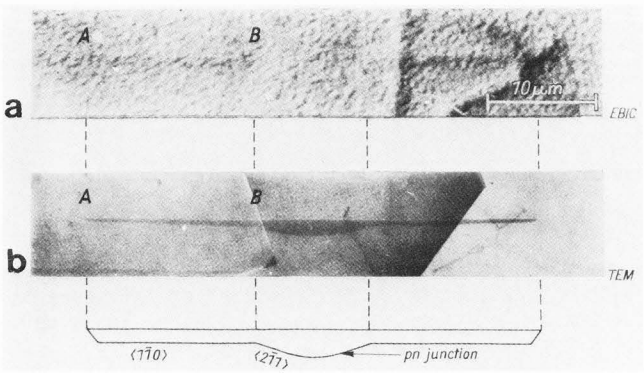

Figure 16. (a) SEM EBIC and (b) TEM 2$\bar{2}$0 strong beam montage of a stacking fault. The Frank partial along the lower edge of the fault varies in EBIC contrast with line orientation. (After Ourmazd and Booker (1979)).

$$\tau' = 1/(N\sigma v_{th}) \quad (15)$$

where v_{th} is the carrier thermal velocity. Combining equations (14) and (15) and introducing the line density of recombination centres

$$N' = N\pi r^2 \quad (16)$$

leads to the expression

$$v = N' \sigma v_{th} \quad (17)$$

If the recombination centres are intrinsic shallow (deformation potential) or deep (dangling bond) states; they will have a line density, of course. The value of v_{th} is known so experimental values of v yield values of the product $N'\sigma$. If a value of σ can be deduced, the value of N' can also be obtained. Kittler and Seifert (1981) used equation (17) to estimate the sensitivity of the EBIC technique. The minimum EBIC contrast observable is 0.05%, which they found to correspond to a value of $v/D = 0.03$, where D is the minority carrier diffusion coefficient. Assuming that the recombination is due to impurities with cross sections $\sigma = 10^{-14}$ cm², they obtained $N'_{min} \gtrsim 200\ \mu m^{-1}$. That is, a dislocation must have at least one impurity recombination centre every 5 nm to give observable EBIC contrast.

Subsequently so-called higher order approximations were introduced into the theory by Pasemann (1981). These concern the use of the actual electron beam injected minority carrier density p instead of the equilibrium value p_0, used as a first approximation by Donalato, in certain of the expressions to be evaluated to obtain the contrast for particular cases. This improved theory is in better quantitative agreement with experiment at a single temperature. An example of the agreement between theoretical and experimental EBIC line scans across a dislocation is shown in Figure 17(b).

The Temperature Dependence of Dislocation EBIC Contrast. Despite its success in accounting for EBIC defect contrast, the Donalato theory and its higher order modifications have limitations. One of these is an inability, without modification, to account for the temperature dependence of dislocation CC contrast. This was shown by the

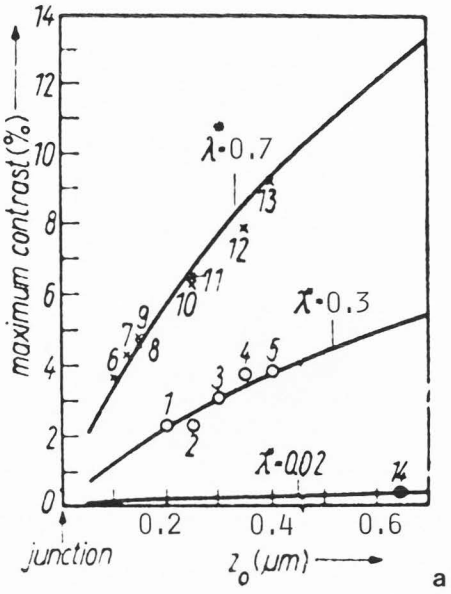

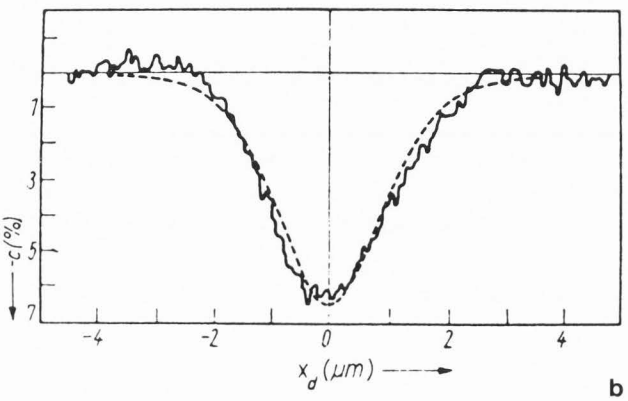

Figure 17 (a) Theoretical curves and experimental points for the variation of dislocation (maximum) contrast with depth for 0 contracted 60° dislocations, x dissociated 60° dislocations and • screw dislocations. (b) Experimental (continuous curve) and theoretical (dashed curve) EBIC contrast profiles of a 60° dislocation in Si. (After Pasemann et al (1982)).

pioneering work of Ourmazd and Booker (1979) and Ourmazd et al (1983a, 1983b) who studied dislocation contrast in EBIC micrographs as a function of the dislocation type and the specimen temperature.

From this point of view, the most important results of the work of Ourmazd and Booker are shown in Figure 18. Ourmazd et al summarise the result of the Donalato theory in the form

$$C = (\pi r^2/\tau')F(L,d,R)$$
$$= v\,F(L,d,R) \qquad (18)$$

where the form of the function F(L,d,R) depends on the experimental geometry. d is the depth of the defect below the beam entry surface and R is the electron penetration range. They therefore measured a normalized contrast:

$$C_n(T) = C/C_{RT} = v/v_{RT} \qquad (19)$$

where C and v are the values for the experimental temperature and C_{RT} and v_{RT} are the room temperature values. Assuming L to be temperature independent, the geometrical function F will be eliminated and the normalized contrast should be the same for all dislocations of the same type. Moreover if two dislocations have the same type of recombination centre but in different concentrations N so the contrast must be written

$$C = N\,v\,F\,(L,\,d,\,R) \qquad (20)$$

the use of the normalized contrast eliminates N also.

Ourmazd et al (1983b) point out the significance of the fact, shown in Figure 18(a), that the normalization of the contrast does not eliminate the differences between different dislocations with the same character. Instead they found that the temperature dependence of the EBIC contrast from different dislocations had the empirical form

$$dC/dT = \alpha\,C_{RT} + \beta \qquad (21)$$

where α and β are constants. Figure 18(b) shows that equation (21) is well obeyed.

This cannot be accounted for by the simple Donalato theory. This was demonstrated by Ourmazd et al (1983b) as follows. Differentiating expression (18) gives

$$dC/dT = (dv/dT)\,F(L,d,R)$$

so

$$\frac{1}{C_{RT}}\frac{dC}{dT} = \frac{1}{v_{RT}}\frac{dv}{dT}$$

i.e.

$$\frac{dC}{dT} = \left(\frac{1}{v_{RT}}\frac{dv}{dT}\right)C_{RT} = \alpha\,C_{RT} \qquad (22)$$

which passes through the origin, as shown in Figure 18(b). This is unaffected by the higher order corrections of Pasemann (1981). Ourmazd et al (1983b) showed that allowing the minority carrier diffusion length to have different values in the bulk and inside the cylinder of influence of the dislocations, instead of assuming it to be constant as in the Donalato theory, leads to a relation of the form (21).

The fact that contrast changes occur well below room temperature indicates that the dislocation recombination levels are shallow. They could therefore be due to shallow-level impurities segregated to the dislocations or to the intrinsic shallow levels arising from the deformation potential of the dislocation. The latter would still arise in the case of dirty dislocations. The deep dangling bond levels would not be expected to show a strong temperature dependence at reduced temperatures in Si and such levels would be eliminated by connecting the dangling bonds to appropriate types of impurity atoms. Parallel work on the CL contrast of dislocations is also making progress (see e.g. Holt and Saba (1985)).

It is clear that EBIC contrast measurements are a powerful means to determine the electrical properties of dislocations and that low temperature measurements are important. Further evidence of this importance will be presented below.

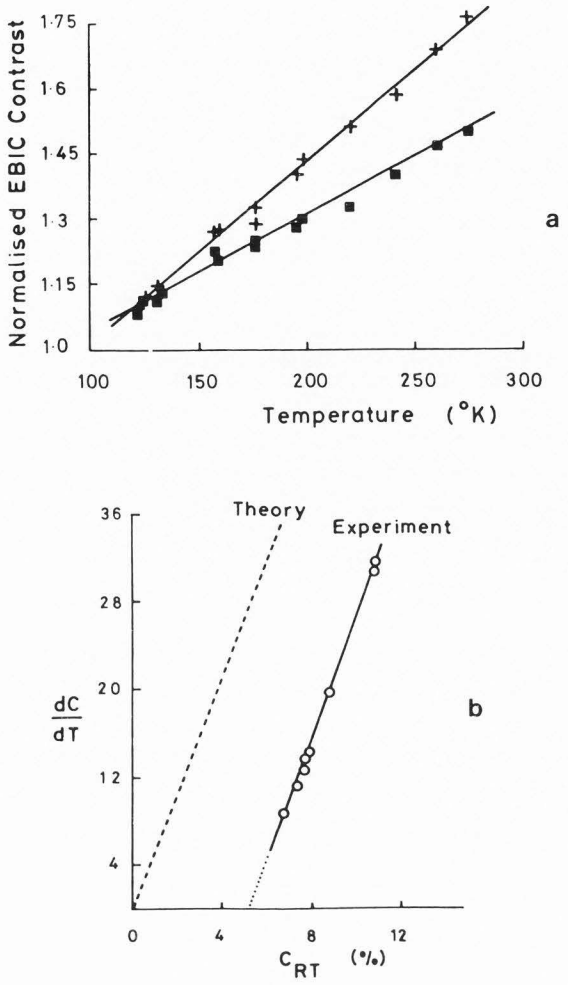

Figure 18. (a) Plot of the normalized EBIC contrast versus temperature for two dislocations (■, +). (b) Plot of the rate of change of EBIC contrast with temperature versus room temperature contrast for a number of different dislocations. (After Ourmazd et al (1983b)).

Grain Boundary Contrast. Interest in the electrical effects of grain boundaries (g.b.s) in Ge and Si arose in the 1950's because they were a problem in the early days of semiconductor crystal growth. In Ge it was found that g.b.s. provided acceptor levels in the energy gap as did dislocations. Consequently g.b.s. had negative surface charges, produced energy band bending and tended to produce local p-type layers in n-type material. The resistance across g.b.s. was high but that along them was low. For a review of the early work on Ge and Si see Sosnowski (1959) and for the theory see Figielski (1960). Interest then largely disappeared to be revived particularly by the interest in polycrystalline Si and other materials for use in low-cost, large area photovoltaic cells for terrestial solar power generation. With g.b.s. as with dislocations a continuing problem is the role of impurity segregation in modifying or controlling the inherent electrical properties of the defect.

Recently, too, powerful new crystallographic theories of grain boundary structures became available. These had been developed through studies of g.b.s. in metals and ceramics (Bollmann (1970), Baluffi et al (1982), Pond and Vlachavas (1983)). Initial applications of the coloured symmetry, group theoretical approach to the analysis of interfaces in semiconductors were published by Pond and Holt (1982), Pond et al (1984) and Holt (1984). This follows from earlier work on the crystallography of grain boundaries in semiconductors (Hornstra (1959, 1960), Holt (1964). Atomic resolution can be applied to observe the core structures of g.b.s. One of the first such micrographs showed a g.b. core structure in Ge predicted by Hornstra (Krivanek et al (1977)). As yet theoreticians have not turned their attention from the quantum mechanics of dislocation cores to that of g.b. cores however.

SEM studies of g.b.s. began with one of the earliest voltage contrast observations showing the occurrence of two p-n junctions back-to-back due to a p-layer at a g.b. in n-type GaP (Alfrey and Wiggins (1960)). These boundaries had been observed to be electroluminescent except for those of the coherent twin boundary type (Holt (1964)). An EBIC micrograph of g.b.s. in GaP is shown in Figure 19. In it can be seen both bright and dark contrast and changes of contrast with orientation. Salerno et al (1981) observed dark, zero and bright contrast at different g.b.s. in CL micrographs of heavily Zn-doped GaAs. Spectral analysis indicated that many of the observed features were due to local variations in impurity concentrations. Russel et al (1980, 1981) used both CC and CL SEM microscopy to examine polycrystalline ZnSe. Bright EBIC contrast was observed at the grain boundaries but not twin boundaries. This was attributed to the effects of engery band bending due to negative charges on the g.b.s.

Recently EBIC line scans across grain boundaries were treated analytically (Seager (1982), Donalato (1983b)). An interface recombination velocity can be obtained in a manner analogous to that used for dislocations as described above.

The electrical inactivity of twin boundaries has been confirmed by several techniques and can be understood in terms both of the lack of dangling bonds in the core of coherent boundaries and of the low elastic strain and hence the lack of impurity segregation to twin interfaces.

A good impression of the interest in the electrical properties of g.b.s., particularly in Si, can be obtained from the proceedings of the 1982 Meeting of the (American) Materials Research Society on Grain Boundaries in Semiconductors and the (French) CNRS International Colloquium on Polycrystalline Semiconductors in 1982, papers from both these are included in references. One of these contains a recent review of the interface state model of grain boundaries and the methods used to measure the density and capture cross section of these states (Broniatowski (1982)). The other contains five papers reporting the results of

EBIC studies (Ast et al (1982), Cunningham et al (1982), Frye and Ng (1982), Paz et al (1982) and Russel et al (1982)). Cunningham et al found that although coherent twin boundaries in Si are electrically inactive, dislocations in such boundaries can act as efficient recombination centres for minority carriers. In this field, too, rapid advances can be anticipated.

Microplasmas in Si Diodes Some recent results are presented here to illustrate one way in which CC measurements at low temperatures can be extended to obtain information about the energy depths of traps.

"Reach through" avalanche photodiodes (APD's) are large Si devices which detect photons in the near infrared by means of the barrier photovoltaic effect. CC mode examination using the EBIC signal thus gives directly relevant information. The structure consists of n^+ and p layers on a π substrate as indicated in Figure 7. They are operated under reverse biases of hundreds of volts which widens the depletion region of the p n^+ junction so it "reaches through" the whole low conductivity π layer. Thus in operation the whole thickness of the device is a high-field region. Carriers generated by photon or electron bombardment will be strongly accelerated. On reaching a sufficiently high energy the electrons produce "impact ionization" and more hole-electron pairs and so on until an "avalanche" of charge carriers results. This device functions in a manner similar to that of the Li-drifted Si detectors used in the energy-dispersive x-ray microanalysers that are fitted to many SEMs.

Localized breakdown can occur prematurely at field-concentrating defects to produce highly undesirable "microplasmas". Figure 20(a) shows a diffusion induced dislocation network near the p n^+ junction and Figure 20(b) shows that, at a high reverse bias, bright microplasmas are produced by the electron beam at a number of nodes of the dislocation network. The ability to observe devices under large reverse biases was essential for this work.

Individual microplasmas occur at precipitates and have characteristic "turn-on" voltages. Well below these voltages they are off and a steady, low current is passed. Well above it they are on i.e. they pass a steady high, avalanche current. Near turn on they are unstable and emit random current pulses which are electrical noise in the device. When the SEM beam is incident on a microplasma site in the unstable state, it is switched on. Consequently microplasma sites appear in bright contrast in Figure 20(b). The effect can be seen in the line scan EBIC records of Figure 21. In Figure 21(a) the bias voltage is well below threshold and the current is stable and varies smoothly. In Figure 21(b) the bias is in the unstable, noise region for the microplasma site at the highest (double) peak near the left hand side. When the beam is incident on this peak the current is stable and high. When the beam is incident elsewhere, thermally triggered noise pulses at the microplasma are added to the locally generated EBIC current giving the noisy, jagged trace. Particular current steps at certain critical voltages in the soft reverse bias current voltage characteristic of noisy APD's were shown to be due to the turn-on of specific microplasmas in this way.

Due to trapped space charge in the microplasma volume, microplasmas have switch-on delay times that are temperature dependent (Nield and Leck (1967), Nuttall and Nield (1975)). At reduced temperatures, in the unstable region just below switch-on, this can result in a fairly regular switching between the on (high current) and off (low current) states as shown in the EBIC line scan trace of Figure 22. Comparing this with Figure 21(b) the current is quiescent (stably on) when the beam scans the microplasma (peak) site. Elsewhere the noise has a constant amplitude. This produces a zig-zag trace of constant height and fairly regular spacing. The temperature dependence of the delay times for switch on after pulsing the voltage up past the turn-on value can be determined. This can be done after a previous avalanche pulse to fill the traps and without such an initial trap filling. This gives information on the trap depths. This technique supplements the well-known capacitance deep level trap spectroscopy. Because the current pulses emitted by avalanching microplasma sites are large, signal strength is not such a problem as it is in scanning deep level spectroscopy (SDLTS) and high spatial resolutions are attainable. It is found that microplasma sites are surrounded by secondary sites and the relative amplitudes of the two types of site are variable. It is not clear how widely applicable such low temperature EBIC methods will prove, but they appear to be worth further exploration.

Computerization of the Electrical Defect Microcharacterization of Integrated Circuits

VLSI (very large scale integrated) circuits may have on the order of 1M components where M in this field is a 'binary Mega' i.e. $2^{20} = 1{,}048{,}576$. The appearance of such circuits will differ radically, not only with the choice of two out of 80 or more pins from which to take the CC signal, but also with the logic state of the circuit and the supply voltage. Detailed interpretation will be complex. If the beam is incident at a point in the interior there will in general be many current paths from the beam impact point to the two CC contacts. These will contain e.g. amplifying transistors and logic gates and they will be interconnected into complex series-parallel networks. The amount and complexity of the micrographic information rapidly obtainable is beyond human interpretive capabilities. Just as CAD (computer aided design) and CAM (computer aided manufacture) have had to be adopted, so too will CAT (computer aided testing). Fortunately, SEM data, including EBIC, but also stroboscopic voltage contrast and OBIC (optical beam induced current), is ideally suited for integration into a complete CADMAT (computer aided design, manufacture and test) system.

To analyse the data produced by SEM inspection, powerful image processing and pattern recognition methods will be necessary. Some initial results of an exploration of a variety of such methods will be reviewed here.

VLSI devices with periodic structures such

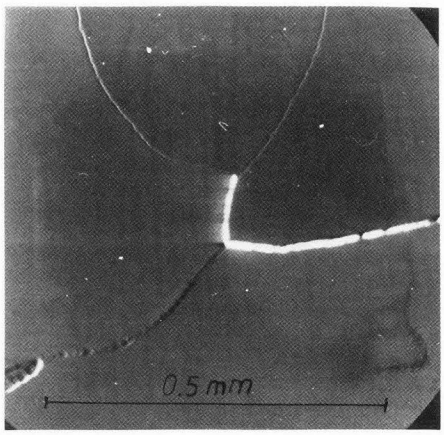

Figure 19. EBIC micrograph of grain boundaries in polycrystalline GaP. (Lesniak, unpublished results).

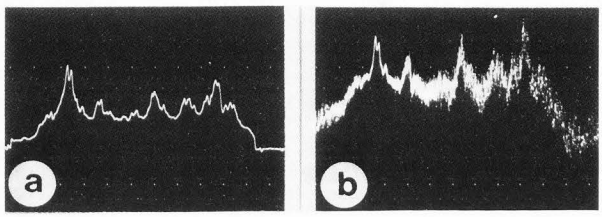

Fig 21. EBIC signal recorded along a line crossing a number of dark lines and microplasma sites in an APD like that of Figure 20 at reverse biases of (a) 360 and (b) 365 V. (After Lesniak and Holt (1983)).

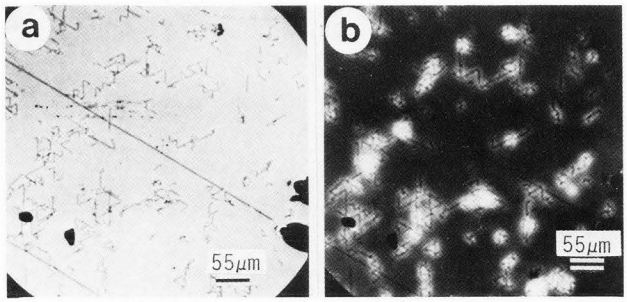

Figure 20. The active junction of a Si avalanche photodiode containing diffusion-induced defects at reverse biases of (a) 0 and (b) 265 V. (After Lesniak et al (1984)).

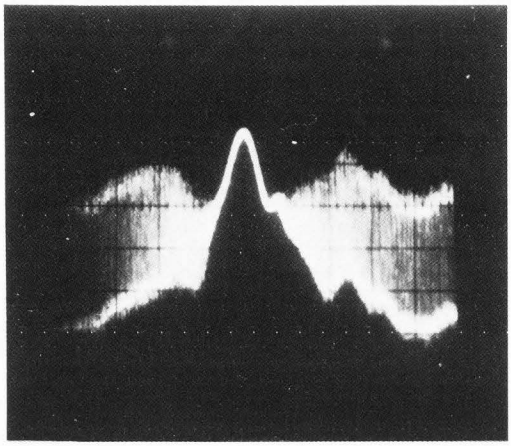

Figure 22. Line scan EBIC trace, at a temperature of 77 K. The microplasma, at the smooth peak position, switched between two current levels except when the beam was incident on the microplasma, when it was continuously "on". (M. Lesniak, unpublished results).

as a memory or a CCD TV (charge coupled device television) sensor will give rise to two dimensional periodic patterns in micrographs. By analogy with TEM it can be understood that the Fourier transform (diffraction pattern) of such a micrograph will be a regular array of spots. Moreover, imperfections in the circuit or device that give contrast in the micrograph, will give rise to effects in the diffraction pattern analogous to those familiar from the selected area diffraction patterns (SADP's) obtained from thin crystals in TEM's. Photographic transparencies were made of SEM CC (EBIC) micrographs of such periodic large scale array devices as shown for example in Figure 23(a). These transparencies were placed in front of a lens and illuminated by a laser. The diffraction patterns recorded in the back focal plane of the lens as e.g. in Figure 23(b) did indeed look much like SADP's from a TEM.

In a laser optical bench it is possible to carry out image processing by "spatial filtering". This requires the production of masks with a pattern of transparent areas designed to transmit only selected parts of the light in the diffraction pattern. By using only the light in the regular array of spots in the diffraction pattern to form a new image via a second lens, the enhancement of clarity of the pattern shown in Figure 23 (c) is obtained. This is the usual purpose of image processing. In the present case, however, the requirement is to filter out the pattern to locate the various forms of imperfection. To do this a photographic negative of the first spatial filter is made. This passes only the light falling outside the spots of the regular array. The image reconstituted from this light does indeed contain only the imperfections as shown in Figure 23(d) (Holt et al (1983)). Thus the first problem in VLSI inspection, that of defect location, is readily solved. The same process

can be carried out by fast Fourier transform (FFT) calculation in a computer. The Fourier transform (FT) of the micrograph, the signal for which is said to be in the time domain, is a Fourier-tranform pattern said to be in the frequency domain. This can be video displayed to obtain a two dimensional pattern much like Figure 23(b). The different points are then described as representing the various frequency components in the micrograph (signal). An obvious method for producing frequency filters to treat such information is to use a micrograph of a good device, compute its Fourier transform and subtract this from the Fourier transform of the device on test. The inverse Fourier transform of the difference is the reconstituted image of the difference between the two original micrographs. This too was found to work (Holt et al (1983)). An obvious extension is to frequency-filter the EBIC micrograph of the device on test with the stored FT computed from CAD data, in order to find the differences between reality and the designer's intention. This method does not depend on periodicity in the VLSI pattern but can be applied to devices and circuits of any form.

In the feasibility studies carried out thus far a few other methods of signal and data processing have been tested. The particular image processing computer we used, a Microconsultants Intellect 200, had facilities for frequency filtering via a simple function with adjustable parameters. The result of the use of such a frequency filter program is illustrated in Figure 24(a). The contrast of the elements of the pattern in the device has been reduced relative to that of the irregular features in the micrograph. By windowing the video signal strength range displayed, i.e. in effect turning down the screen brightness, only the points of excessive EBIC current strength (above a certain threshold, or within a certain range) can finally be imaged as shown in Figure 24(b).

Another approach that immediately occurs to microscopists is electronic processing of the video signal to modify the contrast before display to record the micrograph. The effectiveness of differentiation applied to an appropriate type of defect is illustrated in Figure 25(b) in comparison with the linearly amplified EBIC micrograph in Fig. 25(a). The horizontal lines of the pattern were also very effectively suppressed. Clearly prior electronic signal processing can be followed by computer image processing of the micrograph. Much work remains to be done in determining the optimum methods or combinations of methods for selective defect location in VLSI circuits and devices. An important form of selection is inherent in the use of CC mode micrographs since only electrically active defects will give rise to contrast.

Once the defects have been located they have to be characterized. In part this will be done by computerized application of the methods of defect identification in terms of their electrical properties determined by the sort of fundamental defect studies outlined above. In addition, consultation with device and circuit designers and the results of CAD simulations will be useful. The practical objective must be the rapid ("real time") classification of the defects located as outlined above. Categorization by type, magnitude and location will indicate the defects causing various types and levels of malfunctioning. Knowledge of the initial materials characterization data and of the processing procedures used in manufacture should then identify the cause of the defects and serve to guide efforts to improve yield and reliability.

The versatility of the SEM with its ability to record e.g. voltage contrast, topography, composition (using electron probe microanalysis (EPMA)), and CL to supplement the information in CC or OBIC micrographs is a great attraction of the instrument. The relative ease with which the video signals lend themselves to computerized image and data processing is the other. This line of development alone appears to have the versatility, resolution and speed to be useful for production line testing in the VLSI plants of the future. Consequently the activity in this field is expanding and will continue to expand rapidly. For reviews of the use of the important stroboscopic voltage contrast technique see Menzel and Kubalek (1981), Wolfgang (1983), Feuerbaum (1983) and Menzel (private communication).

OBIC Microscopy for Metal Oxide Semiconductor (MOS) Integrated Circuits

The CC mode and the EBIC method in particular have a drawback for applications to VLSI problems. This arises because virtually all VLSI devices and circuits employ MOS structures. Electron bombardment results in charging of the oxide, destroys the value of the device and would alter the logic state under examination. The charging can be minimized by the use of appropriate conditions such as high beam voltages and low currents and raised specimen temperatures. It can be avoided altogether, in principle, by adopting the method sometimes referred to as SOMSEM OBIC (scanning optical microscopy in an SEM - optical beam induced current).

This method has been demonstrated to be feasible (Maher (1983)). A layer of a phosphor is scanned by the electron beam. The resultant scanning light emitting spot is focussed onto the surface of the circuit below by a lens. The light spot scanning over the surface of the specimen induces barrier and bulk photovoltaic effects and if the short circuit current is detected a true "OBIC" signal is obtained. In principle an optical beam induced voltage (OBIV) method employing the open circuit voltage as signal is also possible. The method is in its infancy but its interest and possible practical importance are obvious.

Multi-technique studies. It is important for the enthusiastic advocates of any technique to recall its limitations. The SEM is less limited than many instruments by virtue of the availability of at least six distinct modes each yielding information about a different group of properties and device parameters. These are the emissive mode (including voltage contrast), the x-ray mode (EPMA), the CC and CL modes, STEM and the recently developed electroacoustic or thermal wave mode. Even so it is important to bear in mind the fact that the SEM is unlikely to be able to solve all problems. Moreover, even if it can, there may be

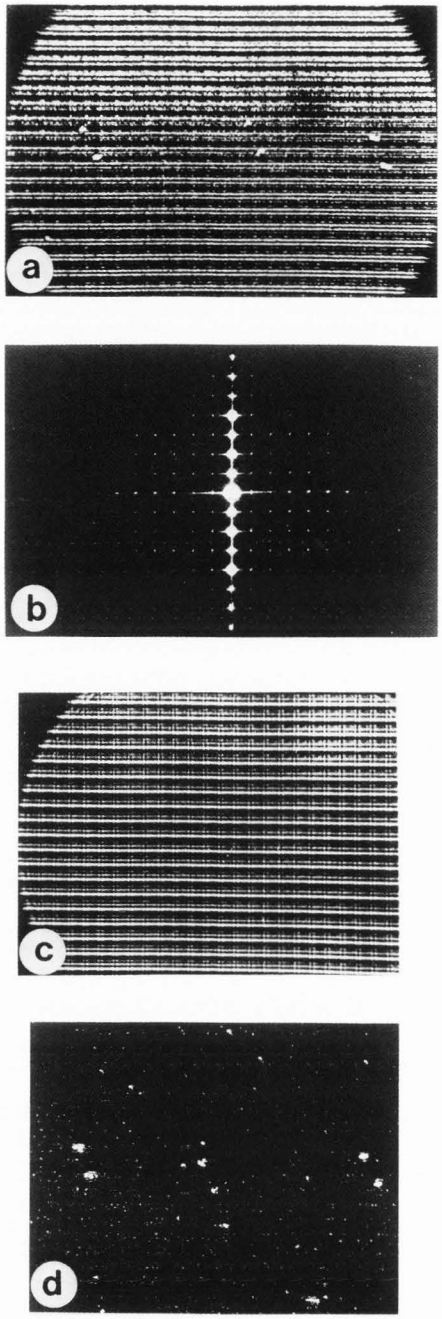

Figure 23. Information on a portion of a large CCD (charge coupled device) TV image sensor. (a) SEM EBIC micrograph. (b) Diffraction pattern of a transparency of (a) produced on a laser optical bench. (c) The reconstituted image produced by spatially filtering out the light other than that in the regular array of spots in (b) and (d) the processed image produced by the light in the diffraction pattern excluded from (c). (After Holt et al (1983)).

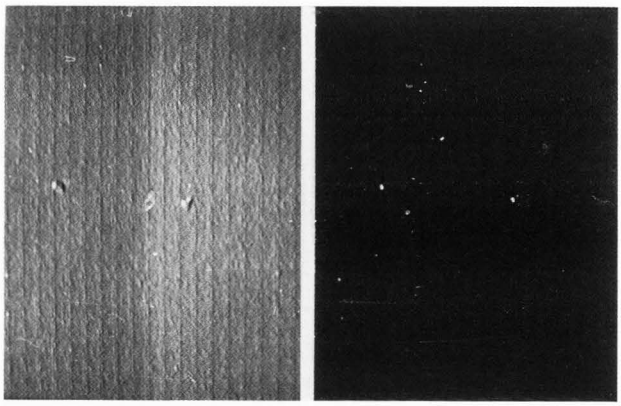

Figure 24. Computer processed SEM EBIC micrograph of an area of a Si CCD image sensor like that in Figure 23(a). (a) Result of use of a real space masking and (b) after additional windowing. (After Luther et al (1984)).

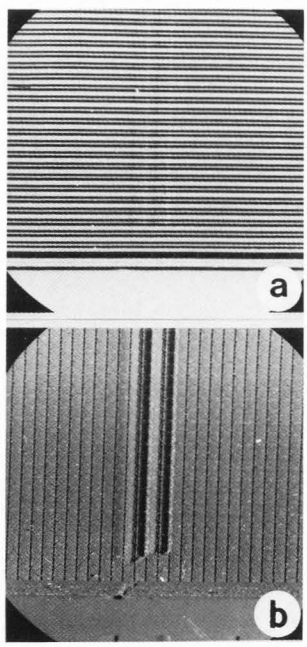

Figure 25. (a) SEM EBIC micrograph of an area of a Si CCD image sensor containing defects blocking charge transfer along two sets of vertical columns. (b) Differentiated and filtered EBIC micrograph of the same area. (After Luther et al (1984)).

more cost effective and quicker methods for getting the same information. The value of etching and light microscopy, x-ray topography, transmission and emission infrared microscopy, and the importance of TEM methods must not be forgotten.

Most industrial problems, even in the semiconductor industry, are relatively simple to recognise (see e.g. the review by Richards and Footner (1983) on failure modes). Many yield and reliability problems still arise from blemishes on masks, insufficient cleanliness in processing, and rough handling of devices. Quick and inexpensive optical examination should generally be the first thing tried.

Acknowledgements

We are grateful to Dr. G.R. Booker for helpful discussions.

References

Alexander, H, Kenn, M, Nordhofen, B, Weber, E, Sander, W. (1975) The EPR Spectra in Silicon with Dislocations, in Lattice Defects in Semiconductors 1974. Conf. Series No. 23, Inst. Phys. London and Bristol, pp.433-438.

Alfrey, G.F.,Wiggins, C.S. (1960) Electroluminescence at Grain Boundaries in Gallium Phosphide, in Solid State Phys. in Electron and Telecomm., (M. Desirant and J.L. Michiels, eds), Academic Press, London, pp.747-750.

Ast, D.G. Cunningham, B. Strunk, H. (1982), EBIC/TEM Investigation of Defects in Solar Cell Silicon, in Grain Boundaries in Semiconductors, (H.J. Leamy, G.E. Pike and C.H. Seager, Eds), Elsevier Sci., New York, pp.167-178.

Balk, L.J. Kubalek, E. Menzel, E. (1974) Untersuch ng von GaAlAs-Elektrolumineszenzdioden im Raster-elecktronenmikroskop. Beitr. elektronenmikroskop. Direktabb. Oberfl. 7, 245-263.

Balk, L.J. Kubalek, E, Menzel, E. (1975). Time-Resolved and Temperature Dependent Measurements of Electron Beam Induced Current (EBIC), Voltage (EBIV) and Cathodoluminescence (CL) in the SEM. Scanning Electron Microsc. 1975: 447-455.

Baluffi, R.W. Brockman, A. King, A.H. (1982) CSL/DSC Lattice Model for General Crystal-Crystal Boundaries and Their Line Defects. Acta Met. 30 1453-1470.

Blenkinsop, I.D. Harding, W.R. Wight, D.R. (1976) Dislocation-Limited Minority Carrier Lifetime in n-type GaP. Electron. Letters 12, 503-504.

Blumentritt, H. Gleichmann, R. Heydenreich, J. Johansen, H. (1979) Combined Scanning (EBIC) and Transmission Electron Microscopic Investigations of Dislocations in Semiconductors. Phys. Stat. Sol. a55, 611-620.

Bollmann, W. (1970) Crystal Defects and Crystalline Interfaces. Springer-Verlag, Berlin.

Bresse, J.F. (1977) Quantitative Use of the Electron Beam Induced Current (EBIC) for the Characterization of Semiconductor Devices. Scanning Electron Microsc. 1977; I:683-693.

Broniatowski, A. (1982) Electrical Measurements of the Grain Boundary Levels in Semiconductors. Colloque C1, supplement to J. de Physique pp. C1-63 to C1-73.

CNRS International Colloquium on Polycrystalline Semiconductors. Proc. Published as J. de Physique. Colloque C1 (1982).

Cunningham, B., Strunk, H.P., Ast, D.G. (1982). The Electrical Activity at Twin Boundaries in Silicon, in Grain Boundaries in Semiconductors, (H.J. Leamy, G.E. Pike and C.H. Seager, eds.), Elsevier Science, New York, pp.51-56.

Czaja, W. (1966). Response of Si and GaP p-n Junctions to a 5 to 40 keV Electron Beam. J. Appl. Phys. 37, 4236-4248.

Davidson, S.M. (1977). Semiconductor Material Assessment by Scanning Electron Microscopy. J. Microscopy 110, 177-204.

Davidson, S.M., Dimitriadis, C.A. (1980). Advances in the Electrical Assessment of Semiconductors using the Scanning Electron Microscope. J. Microscopy 118, 275-290.

Davidson, S.M., Innes, R.M., Lindsay, S.M. (1982). Injection and Doping Dependence of SEM and Scanning Light Spot Diffusion Length Measurements in Silicon Power Rectifiers. Sol. State. Electron. 25, 261-272.

Donalato, C. (1978/79). On the Theory of SEM Charge-Collection Imaging of Localized Defects in Semiconductors. Optik 52, 19-36.

Donalato, C. (1979a). Contrast and Resolution of SEM Charge-Collection Images of Dislocations. Appl. Phys. Lett. 34, 80-81.

Donalato, C. (1979b). Contrast Formation in SEM Charge-Collection Images of Semiconductor Defects. Scanning Electron Microsc. 1979; I:257-266, 274.

Donalato, C. (1979c). Spatial Resolution of SEM-EBIC Images. Sol. State Electron. 22, 797-799.

Donalato, C. (1980). Quantitative Properties of SEM-EBIC Images of Stacking Faults in Silicon. Japan. J. Appl. Phys. 19, L771-L774.

Donalato, C. (1981). EBIC Image Profiles of Dislocations in the STEM. Microscopy of Semiconducting Materials 1981. Conf. Series No. 60, (A.G. Cullis and D.C. Joy, eds.), Inst. Phys. Bristol and London, pp.215-220.

Donalato, C. (1983a). Quantitative Evaluation of the EBIC Contrast of Dislocations. Colloque C4, supplement to J. de Physique 44, C4-269 to C4-275.

Donalato, C. (1983b). Theory of Beam Induced Current Characterization of Grain Boundaries in Polycrystalline Solar Cells. J. App. Phys. 54, 1314-1322.

Donalato, C., Klann, H. (1980). Computer Simulation of SEM Electron Beam Induced Current Images of Dislocations and Stacking Faults. J. Appl. Phys. 51, 1624-1633.

Fathy, D., Sparrow, T.G., Valdre, U. (1980). Observation of Dislocations and Microplasma Sites in Semiconductors by Direct Correlations of STEBIC, STEM and ELS. J. Microscopy 118, 263-273.

Feuerbaum, H.P. (1983). Electron Beam Testing: Methods and Applications. Scanning 5, 14-24.

Figielski, T. (1960). Electronic Processes at Intercrystalline Barriers in Germanium. Acta Phys. Polonica 19, 607-630.

Frye, R.C., Ng, K.K. (1982). Surface Mobilities in Laser-Processed Polysilicon Films, in Grain Boundaries in Semiconductors, (H.J. Leamy, G.E. Pike and C.H. Seager, eds). Elsevier Science New York, pp. 275-286.

Georges, A., Fournier, J.M., Gonchond, J.P., Bois, D. (1980). Time Resolved EBIC for Quantitative Analysis in p-n Junctions. Scanning Electron Microsc. 1980; IV:69-76.

Gopinath, A. (1970). On Scanning-Electron-Microscope Conductive Mode Signals in Semiconductor Devices: Linear Geometry. J. Phys. D. Appl. Phys. 3, 467-472.

Gopinath, A., De Monts De Savasse, T. (1971). On Scanning Electron Microscope Conductive Mode Signals in Bulk Semiconductor Devices: Annular Geometry. J. Phys. D. Appl. Phys. 4, 2031-2038.

Grazhulis, V.A., Osipiyan, Yu. A. (1970). Electron Paramagnetic Resonance in Plastically Deformed Silicon. Sov. Phys. JETP 31, 677-679.

Grazhulis, V.A., Osipiyan, Yu. A. (1971). Electron Paramagnetic Resonance of Dislocations in Silicon. Sov. Phys. JETP 33, 623-628.

Heggie, M.I., Jones, R. (1983). Energy Levels and Properties of Defects on Reconstructed Dislocations in Silicon. Colloque C4, Supplement to J. de Physique 44, pp.C4-43 to C4-47.

Holt, D.B. (1964). Grain Boundaries in the Sphalerite Structure. J. Phys. Chem. Solids 25, 1385-1395.

Holt, D.B. (1974). Quantitative Conductive Mode Scanning Electron Microscopy, in Quantitative Scanning Electron Microscopy, (D.B. Holt, M.D. Muir, P.R. Grant and I.M. Boswarva, eds.), (Academic Press: London), pp.335-386.

Holt, D.B. (1979). Device Effects of Dislocations. Colloque C6, supplement to J. de Physique 40, pp. C6-189 to C6-199.

Holt, D.B. (1981). Recent Developments in SEM Detection Systems for the Cathodoluminescence and Conductive Modes, in Microscopy of Semiconducting Materials 1981. Conf. Series No. 60, (A.G. Cullis and D.C. Joy, eds), (Inst. Phys. : Bristol and London), pp.165-178.

Holt, D.B. (1984). Polarity Reversal and Symmetry in Semiconducting Compounds with the Sphalerite and Wurtzite Structures. J. Mat. Sci. 19, 439-446.

Holt, D.B., Chase, B.D. (1973). Scanning Electron Microscope Studies of Electroluminescent Diodes of GaAs and GaP II Analysis of GaAs Line Scan Traces. Phys. Stat. Sol. a20, 135-144.

Holt, D.B., Culpan, M. (1970). Scanning Electron Microscope Studies of Striations in ZnS. J. Mat. Sci. 5, 546-556.

Holt, D.B., Saba, F.M. (1985). The CL Mode - A Powerful Microcharacterization Technique. Scanning Electron Microsc. 1985 (in press).

Holt, D.B., Lesniak, M., Luther, P. (1983). Image Processing of SEM Micrographs of Integrated Circuits for Defect Location. J. Mat. Sci. Letters 2 565-569.

Hornstra, J. (1959). Models of Grain Boundaries in the Diamond Lattice I. Tilt about <110>. Physica 25, 409-422.

Hornstra, J. (1960). Models of Grain Boundaries in the Diamond Lattice II. Tilt about <001> and Theory. Physica 26, 198-208.

Huang, H.C.W., Aliotta, C.F., Ho, P.S. (1982). Schottky Barrier Height Measurement by Electron-Beam Induced Voltage. Appl. Phys. Lett. 41, 54-56.

Hunter, D.R., Paxman, D.H., Burgess, M, Booker, G.R. (1973). Use of the SEM for Measuring Minority Carrier Lifetimes and Diffusion Lengths, in SEM 1973: Systems and Applications. Conf. Series No. 18, Inst. Phys. Bristol and London, pp.208-213.

Kimerling, L.C., Leamy, H.J., Patel, J.R. (1977). The Electrical Properties of Stacking Faults and Precipitates in Heat Treated Dislocation Free Czochralski Silicon. Appl. Phys. Lett. 30, 217-219.

Kittler, M., Seifert, W. (1981). On the Sensitivity of the EBIC Technique as Applied to Defect Investigations in Silicon. Phys. Stat. Sol. 66a, 573-583.

Krivanek, O.L., Isoda, S., Kobayashi, K. (1977). Lattice Imaging of a Grain Boundary in Crystalline Germanium. Phil. Mag. 36, 931-940.

Labusch, R., Schroter, W. (1980). Electrical Properties of Dislocations in Semiconductors, in Dislocations in Solids Vol. 5, (F.R.N. Nabarro, ed.), North Holland, Amsterdam, pp. 127-191.

Leamy, H.J. (1982). Charge Collection Scanning Electron Microscopy. J. Appl. Phys. 53, R51-R80.

Lesniak, M., Holt, D.B. (1983). Electrically Active Defects in Si Photodetector Devices. Microscopy of Semiconducting Materials 1983, Conf. Series No. 67, (A.G. Cullis, S.M. Davidson and G.R. Booker, eds), Inst. Phys., Bristol and London pp. 439-444.

Lesniak, M., Unvala, B.A., Holt, D.B. (1984). An Improved Detection System for Electrical Microcharacterization in a Scanning Electron Microscope. J. Microscopy 135, 255-274.

Luther, P., Holt, D.B., Lesniak, M. (1984). Defect Analysis of Integrated Circuits, in Electron Microscopy and Analysis 1983, Conf. Series No. 68, (P. Doig, Ed), Inst. Phys., Bristol and London, pp.235-238.

MacDonald, N.N., Everhart, T.E. (1965). Direct Measurement of the Depletion Layer Width Variation vs. Applied Bias for a p-n Junction. Appl. Phys. Lett. 7, 267-269.

Maher, E.F. (1983). Scanning Optical Microscopy with the SEM, in Electron Microscopy and Analysis 1983, Conf. Series No. 68, (P. Doig, Ed.), Inst. Phys., Bristol and London, pp.503-506.

Marklund, S. (1983). Structure and Energy Levels of Dislocations in Silicon. Colloque C4. Supplement to J. de Physique 44 pp. C4-25 to C4-35.

Marten, H.W., Hildebrand, O. (1983). Computer Simulation of EBIC Linescans across p-n Junctions Scanning Electron Microsc. 1983; III:1197-1209.

Menzel, E., Kubalek, E. (1981). Electron Beam Test Techniques for Integrated Circuits. Scanning Electron Microsc. 1981; I:305-322.

Munakata, C. (1966). On the Voltage Induced by an Electron Beam in a Bulk Semiconductor. Japan. J. Appl. Phys. 5, 756-763.

Munakata, C. (1967a). Detection of Resistivity Variation in a Semiconductor Pellet with an Electron Beam. Microelectronics and Reliability 6, 27-33.

Munakata, C. (1967b). An Electron Beam Method of Measuring Resistivity Distribution in Semiconductors. Japan. J. Appl. Phys. 6, 963-971.

Munakata, C. (1968a). Voltage Signal due to Electron-Beam-Induced Conductivity in Semiconductors. Japan. J. Appl. Phys. 7, 1051-1055.

Munakata, C. (1968b). An Application of Beta Conductivity to Measurement of Resistivity Distribution. J. Phys. E. 1, 639-642.

Munakata, C. (1969). Scanning Electron Micrograph using Beta-Conductive Signal. J. Phys. E. 2, 738.

Nield, M.W., Leck, J.H. (1967). A Report on the Delay Time of an Avalanche Discharge in Silicon. Brit J. Appl. Phys. 18, 185-191.

Nuttall, K.I., Nield, M.W. (1975). An Investigation into the Behaviour of Trapping Centres in Microplasmas. Sol. State Electron. 18, 13-23.

Ourmazd, A., Booker, G.R. (1979). The Electrical Recombination Efficiency of Individual Dislocations and Stacking Fault Defects in n-Type Silicon. Phys. Stat. Sol. (a)55, 771-784.

Ourmazd, A., Weber, E., Gottschalk, G.R., Alexander, H. (1981). The Electrical Behaviour of Individual Screw and 60° Dislocations in n-type Silicon, in Microscopy of Semiconducting Materials 1981, Conf. Series No. 60, (A.G. Cullis and D.C. Joy, eds.), Inst. Phys., Bristol and London, pp. 63-68.

Ourmazd, A., Wilshaw, P.R., Booker, G.R. (1983a) The Electrical Behaviour of Individual Dislocations, Shockley Partials and Stacking Fault Ribbons in Silicon. Physica 116B, 600-605.

Ourmazd, A., Wilshaw, P.R., Booker, G.R. (1983b). The Temperature Dependence of EBIC Contrast from Individual Dislocations in Silicon. Colloque C4, supplement to J. de Physique 44, pp.C4-289 to C4-295.

Pasemann, L. (1981). A Contribution to the Theory of the EBIC Contrast of Lattice Defects in Semiconductors. Ultramicroscopy 6, 237-250.

Pasemann, L., Blumentritt, H., Gleichmann, R. (1982). Interpretation of the EBIC Contrast of Dislocations in Silicon. Phys. Stat. Sol. a70, 197-209.

Paz, O., Bhat, K.N., Borrego, J.M. (1982). Charge Collection Characterization of Polycrystalline n-GaAs Layers for Solar Cells, in Grain Boundaries in Semiconductors, (H.J. Leamy, G.E. Pike and C.H. Seager, Eds.), Elsevier Sci. New York, pp. 223-228.

Petroff, P.M., Lang, D.V., Strudel, J.L., Logan, R.A. (1978). Scanning Transmission Electron Microscopy Techniques for Simultaneous Electronic Analysis and Observation of Defects in Semiconductors. Scanning Electron Microsc. 1978; I:325-332.

Petroff, P.M., Logan, R.A., Savage, A. (1980). Nonradiative Recombination at Dislocations in III-V Compound Semiconductors. Phys. Rev. Letters 44, 287-291.

Pond, R.C., Holt, D.B. (1982) Antisymmetry of Surfaces and Interfaces in Polar Materials. Colloque C1, supplement to J. de Physique 43, pp.C1-57 to C1-62.

Pond, R.C., Vlachavas, D.S. (1983). Bicrystallography. Proc. R. Soc. Lond. A386, 95-143.

Pond, R.C., Gowers, J.P., Holt, D.B., Joyce, B.A., Neave, J.H. Larsen, P.K. (1984). A General Treatment of Antiphase Domain Formation and Identification at Polar-Nonpolar Semiconductor Interfaces. Mat. Res. Soc. Symp. Proc. Vol. 25, (1984), 273-278.

Richards, B.P., Footner, P.K. (1983). Failure Analysis in Semiconducting Devices-Rationale, Methodology and Practice. G.E.C. J. Res. 1, 74-91.

Russel, G.J., Robertson, M.J., Vincent, B., Woods, J. (1980). An Electron Beam Induced Current Study of Grain Boundaries in Zinc Selenide J. Mat. Sci. 15, 939-944.

Russel, G.J., Waite, P., Woods, J. (1981). Electrically Active Grain Boundaries in Polycrystalline Zinc Selenide, in Microscopy of Semiconducting Materials 1981, Conf. Series no. 60, (A.G. Cullis and D.C. Joy, Eds.), Inst. Phys., Bristol and London, pp.371-376.

Russel, P.E., Herrington, C.R., Burke, D.E., Holloway, P.H. (1982). The Effect of Heat Treatment on Grain Boundary Properties in Cast Polycrystalline Silicon, in Grain Boundaries in Semiconductors, (H.J. Leamy, G.E. Pike and C.H. Seager, Eds.), Elsevier Sci. New York, pp. 185-191.

Salerno, J.P., Gale, R.P., Fan, J.C.C., Vaughan, J. (1981). Scanning Cathodoluminescence Microscopy of Polycrystalline GaAs, in Defects in Semiconductors, (J. Narayanan and T.Y. Tan, Eds.) North Holland, New York, pp.509-514.

Schick, J.D. (1981) Electron Beam Induced Current Analysis of Integrated Circuits. Scanning Electron Microsc. 1981; I:295-304.

Schick, J.D. (1985). Advances in Electron Beam Induced Current Analysis of Integrated Circuits. Scanning Electron Microsc. 1985; I: 55-66.

Schmidt, U., Weber, E., Alexander, H., Sander, W. (1974). On the Magnetic Properties of Dislocations in Silicon. Sol. State Commun. 14, 735-739.

Schroter, W. (1980). Electric and Dynamic Properties of Dislocations in the Elemental and Compound Semiconductors, in Electronic Structure of Crystal Defects and Disordered Systems, (Summer School, Aussois, 1980), (F. Gautier, M. Gerl and P. Guyot, Eds.), Les Editions Physique, Les Ulis Cedex, pp.129-174.

Schroter, W., Scheibe, E., Schoen, H. (1980). Energy Spectra of Dislocations in Silicon and Germanium. J. Microscopy 118, 23-34.

Seager, C.H. (1982). The Determination of Grain Boundary Recombination Rates by Scanned Spot Excitation Methods. J. Appl. Phys. 53, 5968-5971.

Shockley, W. (1953). Dislocations and Edge States in the Diamond Crystal Structure. Phys. Rev. 91, 228.

Sosnowski, L. (1959). Electronic Properties at Grain Boundaries, J. Phys. Chem. Solids 8, 142-146.

Toth, A.L. (1981). Measurement of EBIC Contrast and Resolution of Dislocations in Silicon. In Microscopy of Semiconducting Materials 1981, Conf. Series No. 60, (A.G. Cullis and D.C. Joy, Eds.), Inst. Phys., Bristol and London, pp.221-222.

Wilshaw, P.R., Ourmazd, A., Booker, G.R. (1983). Some Aspects of the Measurements of Electrical Effects of Dislocations in Silicon using a Computerized EBIC System. Colloque C4, Supplement to J. de Physique 44, pp.C4-445 to C4-450.

Wittry, D.B., Kyser, D.F. (1965). Cathodoluminescence at p-n Junctions in GaAs. J. Appl. Phys. 36, 1387-1389. PL64.

Wolfgang, E. (1983). Electron Beam Testing: Problems in Practice. Scanning 5, 71-83.

Zimmermann, W. (1972). Measurement of Spatial Variations of the Carrier Lifetime in Silicon Power Devices. Phys. Stat. Sol. (a)12, 671-678.

List of Symbols

A_d diode area
A^* Richardson constant
C Contrast
D minority carrier diffusion coefficient.
e the charge on an electron
e; the "ionization energy" of the material i.e. the effective average value of the energy to form a hole-electron pair.
ε the dielectric constant.
F geometrical function appearing in the Donalato contrast theory.
$\emptyset_B$ the Schottky barrier height.
G the generation factor i.e. the number of hole-electron pairs produced per incident electron.
I_a the actual value of I(x) for x=o.
I_b the beam current.
I_B the value of I_{sc} with the beam incident on defect-free bulk material.
I_D the value of I_{sc} with the beam incident on a defect.
I_g the current generated in the specimen by the beam.
I_j the junction current back through a barrier.
I_m the extrapolated value of I(x) for x = o.
I_o the saturation reverse bias current of a rectifying diode.
I(o) the initial, steady value of I_{sc} at t = 0, when the beam was cut off.
I_{sc} the short circuit current (true EBIC signal) due to a barrier or bulk electron voltaic effect.
I(t) the value of I_{sc} a time t after chopping the beam.
I(x) the value of I_{sc} for a beam to barrier distance x.
k the Boltzmann constant.
K the backscattering coefficient i.e. the fraction of beam electrons that are back scattered.
n ideality factor of a barrier.
N (volume) density of recombination centres in the cylinder of influence round a dislocation.
N' (line) density of recombination centres in the cylinder of influence round a dislocation.
N_A acceptor density.
η_{cc} charge collection efficiency of a barrier.
r radius of the cylinder of influence round a dislocation, within which the minority carrier lifetime is reduced.
σ capture cross-section of the recombination centres associated with a dislocation.
τ minority carrier lifetime.
τ' reduced minority carrier lifetime in the cylinder of influence round a dislocation.
v line recombination velocity (index of recombination "strength" or "efficiency") of a dislocation.
v_{th} thermal velocity of the minority carriers.
V_a applied voltage.
V_b the beam voltage.
V_d the diffusion potential drop across e.g. p-n junction.
V_{oc} the open circuit voltage (true EBIV signal) due to a barrier or bulk electron voltaic effect.

Discussion with Reviewers

J.D. Schick: You mention beam-chopping and phase-lock systems. What application utilizes this approach and what advantages and/or disadvantages might be gained by beam-chopping techniques?
Authors: So far as we are aware nobody has tried to compare beam-chopping and phase-lock amplification with other methods. The obvious advantage of the method is, of course, that the noise occurring in the absence of beam bombardment can be subtracted. In our experience there is no difficulty in backing off the steady "dark" background currents in the cases we have studied. Something like the phase-lock method would be necessary if dark noise of large amplitude relative to the signals were encountered. This is unlikely to happen in well developed materials and devices because the generation factor G is so large that the CC signals tend to be well above specimen noise levels. This might not be the case, however, for example for β-conductivity signals from semi-insulating GaAs. We are beginning to make such observations but so far have not experienced this difficulty.

J.D.Schick: In charge collection measurements, such as those performed by Huang et al (1982) where there is a grain structure associated with a metal film through which the electron beam energy is penetrating to excite the signal, how is the variation in signal due to the variation in absorbed energy accounted for?
Authors: Neither Huang et al (1982), nor any other published work of which we are aware, attempts to make such a correction.

J.D. Schick: In the case where trap depth information is obtained from temperature dependence (it seems to be like what are sometimes referred to as thermally stimulated conductivity measurements) are the traps referred to physically located at the defect where the microplasma takes place or throughout the bulk material?
Authors: The measurements concern the contrast due, for example, to dislocations and the spatial resolution is that of the CC mode, i.e., of the order of a μm. The question whether intrinsic dislocation levels have been detected or whether the observed effects are due to point defect segregation is at present an open one. In most published work it is clear that the large contrast often seen, of the order of a 10% reduction in EBIC signal, is due to segregation. The observation of smaller contrast, of the order of 1% at presumably cleaner dislocations may or may not be due to intrinsic dislocation recombination centres.

J.D. Schick: You mention the use of an internal head amplifier and you discuss switching connections among many possible connecting points in a chip. How is this switching accomplished outside of the vacuum system of the SEM?
Authors: Miniature sealed relays could be used inside the specimen chamber. Dr. S. Davidson (private communication) has successfully used a ribbon cable to an external plug board.

J.D. Schick: In your last statement you mention that "most industrial problems are relatively simple to recognize..." Many of the semiconductor device/circuit failure analyses that I perform or witness are pushing the technology capability involved near to their limit already. They may be simple, but they are not easy.
Authors: I am well aware that many industrial problems, especially those arising at the frontier of development of new materials, new devices and larger scales of integration are extremely challenging. Your own work indeed exemplifies this most impressively. What I was referring to was the frequent recurrence, possibly with minor variations, on many processing lines, of well known phenomena such as "cosmetic" defects (visible blemishes) due to dust or scratches on reticles, microplasmas, diffusion shorts and other soft junction phenomena due to contamination, etc. I understand that many such problems are solved by visual examination or etching and light microscopy plus experience and "good housekeeping" on the production line.

G. Koschek: Please comment on the attainable spatial resolutions of the mentioned CC-modes especially EBIC/EBIV.
Authors: The spatial resolution of the CC mode techniques is not entirely understood. In principle the incident beam diameter, the electron penetration range and the minority carrier diffusion length should all help to determine it. In practice the resolution is generally found to be about equal to the penetration range (and so beam voltage dependent). The beam diameter is usually negligible by comparison, but why little dependence on diffusion length is found is not entirely clear.

G. Koschek: A very important new method for microcharacterization using the CC-mode of the SEM is scanning deep level transient spectroscopy, which you merely mention by one sentence. Could you comment on this method more comprehensively, especially the possibilities for microcharacterization of suitable materials e.g. semiconductors or electronic ceramics?
Authors: The scanning deep level transient spectroscopy technique should be an extremely powerful one as it would combine spatial resolution with the well-known advantages of deep level trap spectroscopy (P.M. Petroff, D.V. Lang, J.L. Strudel and R.A. Logan (1978) Scanning Transmission Electron Microscopy Techniques for Simultaneous Electronic Analysis and Obervation of Defects in Semiconductors. Scanning Electron Microsc. 1978; I: 325-332). Its use has been inhibited by the weakness of the signals. The recent development of a more sensitive detector (O. Breitenstein (1982) A Capacitance Meter of High Absolute Sensitivity Suitable for Scanning DLTS Application. Phys. Stat. Sol. a71, 159) appears to have made the method more widely applicable. As yet few results have appeared but several groups are known to be working in this field.